Plasmonics (2025) 20:10613–10623
https://doi.org/10.1007/s11468-025-03136-8

RESEARCH

Annular Bore Array H-Type PCF-SPR Sensor with High Sensitivity

Fengrui Yang[1] · Wei Liu[1] · Jianxin Wang[1] · Jingwei Lv[1] · Famei Wang[2] · Zao Yi[3] · Qiang Liu[1] · Paul K. Chu[4] · Chao Liu[1]

Received: 20 May 2025 / Accepted: 18 June 2025 / Published online: 2 July 2025

Abstract
Photonic crystal fibre (PCF) sensors, based on the principle of surface plasmon resonance (SPR), have broad application prospects in many fields such as biomedical sensing, food safety detection and chemical sensing. However, although many PCF-SPR sensors have been proposed, their complex structures, difficult preparation and poor sensing performance have severely limited the further development of this technology. In order to effectively reduce the difficulty of fibre preparation and improve its practicality, this paper designs a high-sensitivity ring-hole array photonic crystal fibre sensor. The sensor is equipped with two layers of ring-hole arrays, the optical fibre is polished into an H-shaped structure, and a gold film is uniformly coated on the polished surface. Simulation analysis shows that this unique structure gives the sensor an ultra-wide detection range and excellent high sensitivity. By optimising the sensor structure, the sensing characteristics have been significantly improved. Specifically, the maximum wavelength sensitivity is up to 34,000 nm/RIU, the average sensitivity is 10,833.3 nm/RIU, the minimum resolution is as low as 2.94×10^{-6} RIU^{-1}, the detectable refractive index range is 1.36–1.42, and the wavelength detection range is 570 to 1300 nm. With the outstanding advantages of simple structure and high sensitivity, this sensor has great potential and value for applications in biomedical sensing, chemical sensing and many other fields.

Keywords Photonic crystal fibre · Surface plasmon resonance · High sensitivity · Ring-hole array

Introduction

Sensing technology is developing rapidly and is one of the three pillars of the information industry, along with communications and computing. Surface plasmon resonance is a physical-optical phenomenon in which free electrons in a metal absorb the energy of incident light and generate electronic oscillations under certain conditions. SPR is characterised by high-sensitivity, real-time monitoring and label-free detection, and is therefore widely used in many fields such as life sciences, environmental monitoring and chemical research [1–4].

PCF not only retains all the advantages of conventional fibre optics but also overcomes their limitations, such as high transmission loss and narrow single-mode wavelength range. It also offers benefits like reduced fibre loss and high non-linearity [5, 6]. The benefits are significant and include cut-off-free single-mode transmission, excellent dispersion, low bending loss, full wavelength transmission and high birefringence [7, 8]. The ability to flexibly adjust the geometry, structural parameters and material properties of PCFs allows researchers to tailor their optical properties to their own needs, which is very convenient for scientific research [9, 10]. PCF-SPR sensors have proven their value in many applications. In the biomedical field, it can detect cancer cells by monitoring changes in the refractive index of cells, which is of great importance for the early prevention and treatment of diseases [11]. In addition, the sensor is widely used in the fields of environmental protection [12], chemical sensing [13], food safety [14] etc., providing powerful technical support for environmental quality monitoring, chemical composition analysis and food quality testing.

✉ Chao Liu
msm-liu@126.com

1 School of Physics and Electronic Engineering, Northeast Petroleum University, Daqing 163318, China

2 Shenzhen Key Laboratory of Ultra-Intense Laser and Advanced Material Technology, Center for Intense Laser Application Technology, and College of Engineering Physics, Shenzhen Technology University, Shenzhen 518118, China

3 Joint Laboratory for Extreme Conditions Matter Properties, Southwest University of Science and Technology, Mianyang 621010, China

4 Department of Physics, Department of Materials Science and Engineering, and Department of Biomedical Engineering, City University of Hong Kong, Tat Chee Avenue, Kowloon, Hong Kong, China

Early SPR sensors were mainly based on prismatic structure design. Although these traditional prismatic SPR sensors have the advantage of stable and reliable performance, they need to be equipped with a large number of mechanical parts in the actual manufacturing process. This leads to obvious limitations in practical applications, such as large size, high manufacturing cost and difficulty to realise remote sensing functions, so it is not suitable for real-time detection and sensing tasks [15, 16].

With the development of technology, fibre optic sensors based on the SPR principle have gradually replaced prismatic SPR sensors as a research hotspot in this field due to the significant advantages of easy miniaturisation, low manufacturing cost and support for real-time detection [17]. Among the fibre optic SPR sensors, the performance of PCF-SPR sensors mainly depends on the plasmonic material and the design of the PCF structure. Gold and silver are the two most commonly used plasmonic materials due to their stable chemical properties.

In 2023, Ammar M. et al. designed a photonic crystal fibre optic sensor with a gold film on its surface [18]. The sensor featured an irregular wavy polishing surface and exhibited a maximum wavelength sensitivity of 17,500 nm/RIU. However, the irregularity of the polishing surface results in an uneven distribution of the gold film on its surface, which in turn affects the sensing efficiency. In 2024, Fei et al. designed a D-type double core with a gold film and ITO coated on the surface of the D-type [19], with a maximum wavelength sensitivity of 22,100 nm/RIU. However, the special structure of the D-type makes it difficult for the fibre to maintain the stability of its optical properties when subjected to external stress or environmental changes, and the efficiency of the abrupt field interactions cannot be guaranteed. In 2024, Luo et al. designed a photonic crystal fibre optic sensor with two elliptically grooved microchannels [20], which can achieve dual-channel measurement with a maximum wavelength sensitivity of 18,000 nm/RIU. However, due to the excessive number of air holes inside and their irregular arrangement, it is very male in the manufacturing process and not easy to integrate and package.

In this study, an innovative ring-hole array photonic crystal fibre optic sensor is designed and systematically analysed using the full vector finite element method. Inside the fibre, two layers of air holes are arranged in a circular array, which are polished to form an H-shaped structure and coated with a gold film on the polished surface. This unique design effectively solves the key problems of poor structural stability, low-speed field propagation efficiency and the difficulty of integration and packaging in actual production. Simulation results show that the sensor has excellent sensing performance. The data show that the sensor can detect refractive indices in the range of 1.36–1.42, with a maximum wavelength sensitivity as high as 34,000 nm/RIU, a resolution as low as 2.94×10^{-6} RIU^{-1}, an optimum quality factor of 316 RIU^{-1} and an ultra-wide wavelength detection range of 570–1300 nm. Based on the above performance advantages, the sensor has a broad application prospect in the fields of biomedicine, chemical sensing and food safety. For example, in the biomedical field, the PCF can be used for early detection of cancer cells by accurately monitoring changes in the refractive index of cells. Table 1 lists the refractive index data of common cells in normal and cancerous states that can be monitored by this PCF sensor, providing strong support for practical applications [21].

Structure and Analysis

Figure 1a and b present the 2D and 3D cross-sectional schematics of the photonic crystal fibre sensor with an annular hole array structure, respectively. In this study, the performance of the sensor was analysed by numerical simulation using COMSOL Multiphysics v6.2 software. During the simulation process, the structural parameters of the sensor are set with a high degree of precision: the fibre radius is 10 μm, the centre aperture radius d_1 is 0.1 μm, the inner aperture radius d_2 is 0.9 μm, the outer aperture radius d_3 is 1.2 μm, and the polishing depth d_4 is 5 μm. Two gold films with thicknesses of 38 nm are symmetrically deposited on the polished surface, using either magnetron sputtering or chemical vapour deposition (CVD) technology. The outermost layer functions as a matching layer, absorbing scattered light during the simulation process and preventing it from influencing the results.

As demonstrated in Fig. 1c, the sensor is affixed to a single-mode optical fibre at both extremities, with the droplets to be measured and analysed being deposited on the surface. In the process of actual detection, the light emitted by the light source is transmitted through the single-mode fibre, which functions as a medium for the transfer of light, and is then coupled into the sensor. The light then undergoes transmission to the spectrometer. The spectrometer is responsible for the collection of data, which are subsequently transferred to a computer for analysis and processing.

Table 1 Refractive indexes of common cells in the normal and cancerous states

Cancer types	Cell types	Refractive indexes of normal cells	Refractive indexes of cancerous cells
Skin	Basal	1.360	1.380
Cervical	Hela	1.368	1.392
Blood	Jurkat	1.376	1.390
Adrenal gland	PC12	1.381	1.395

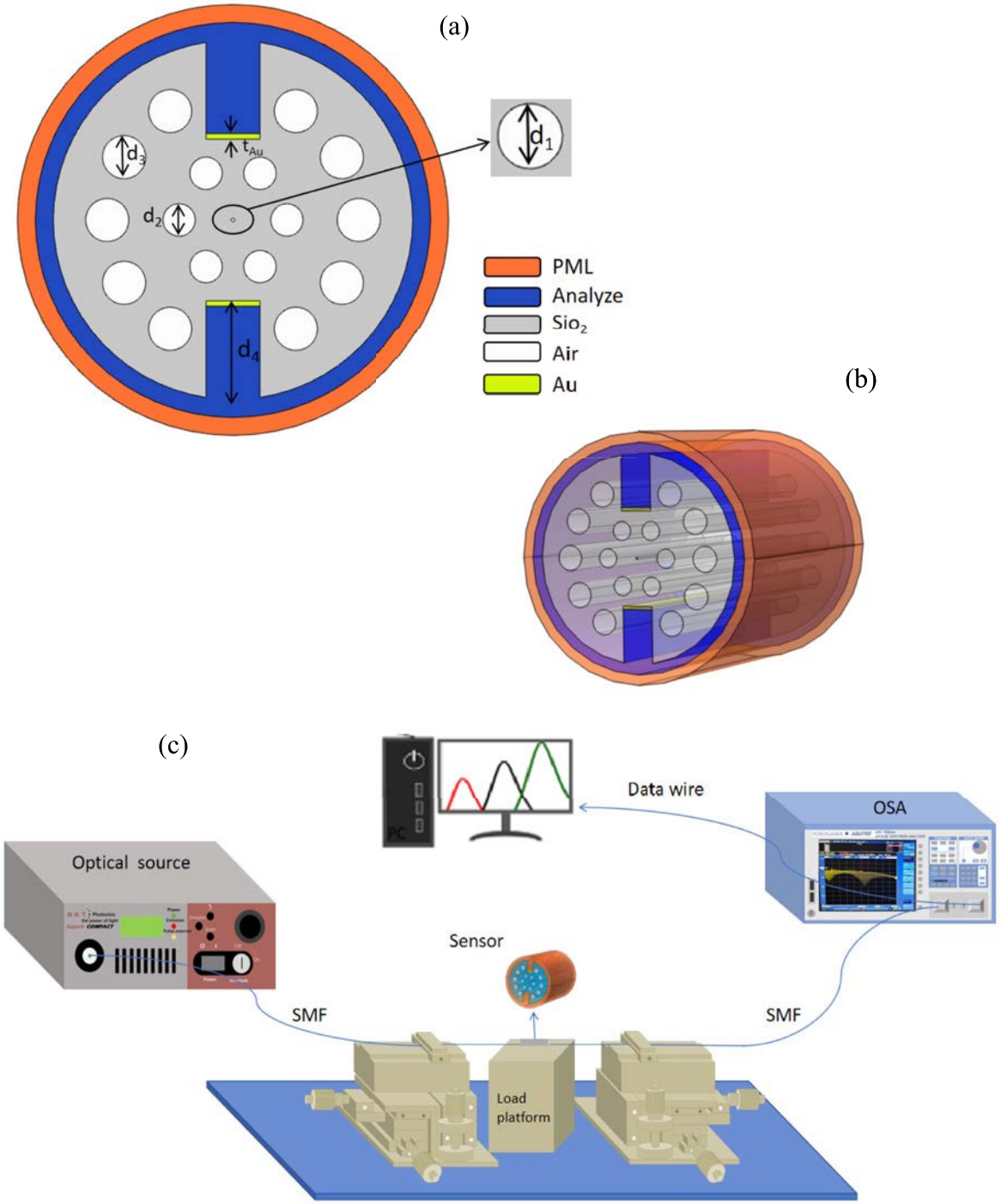

Fig. 1 **a** Cross-section of the sensor; **b** three-dimensional view of the sensor; **c** schematic diagram of the experimental setup

In this study, the finite element method is utilised to systematically analyse the sensor characteristics. The primary material of the sensor is silicon dioxide, and the refractive index of this material is wavelength-dependent. The value of this index can be calculated with high accuracy using the Sellmeier dispersion relation [22]:

$$n^2_{Silica} - 1 = \frac{A_1\lambda^2}{\lambda^2 - B_1^2} + \frac{A_2\lambda^2}{\lambda^2 - B_2^2} + \frac{A_3\lambda^2}{\lambda^2 - B_3^2} \quad (1)$$

This equation has the capacity to comprehensively delineate the optical dispersion characteristics of silicon dioxide across a range of wavelengths. Consequently, it provides a

theoretical foundation for the precise determination of the material's optical parameters within the finite element simulation. This, in turn, ensures the reliability and accuracy of the sensor performance analysis outcomes. The values of A1, A2, A3, B1, B2 and B3 are as follows: A1 = 0.6961663, A2 = 0.4079426, A3 = 0.8974794, B1 = 0.0684043, B2 = 0.1162424 and B3 = 9.896161.

The dielectric constant of gold can be determined by means of the Drude-Lorentz model [23]:

$$\varepsilon_{Au} = \varepsilon_{\infty} - \frac{\omega_D^2}{\omega\left(\omega + i\gamma_D\right)} - \frac{\Delta\varepsilon \cdot \Omega_L^2}{\left(\omega^2 - \Omega_L^2\right) + i\Gamma_L\omega} \tag{2}$$

In this text, the symbol ε_{Au} is employed to denote the dielectric constant of gold. The high-frequency dielectric constant, denoted ε_{∞}, is specified as 5.9673. The value of the weighing factor is thus determined to be equal to 1.09 times the unit of angular frequency, denoted here by the letter "ω". The plasma frequency, denoted here by the letter "ω_D", and the damping frequency, denoted here by the letter "γ_D", are thus defined as the values of the corresponding functions. The term "Ω_L" is an abbreviation for "oscillator strength", and "Γ_L" is an abbreviation for "spectral width". The specific values of the aforementioned quantities are as follows: $\omega_D = 4227.2\pi$ THz, $\gamma_D = 31.84\pi$ THz, $\Omega_L = 1300.14\pi$ THz and $\Gamma_L = 209.72\pi$ THz.

Results and Discussion

Subsequent to the finalisation of the preliminary structural design, a systematic optimisation process was initiated for the primary structural parameters of the sensor. The initial step in this process is the precise calibration of the thickness of the gold film. In accordance with the principles of surface plasmon resonance (SPR), when light waves are transmitted along an optical fibre and interact with a metal film layer, the free electrons within the metal film generate collective oscillations due to excitation by the electromagnetic field of the light wave. These oscillations in turn excite the surface plasma wave. As the core medium for energy conversion, the thickness of the gold film has a direct impact on the energy coupling efficiency between the photonic crystal fibre. Minor alterations to the film thickness can therefore have a substantial effect on the performance of the sensor.

During the optimisation process, eight discrete parameters (ranging from 26 to 40 nm) were selected for study, since the sensor is unable to effectively stimulate the SPR effect when the gold film is thinner than 26 nm or thicker than 40 nm. The loss spectral data shown in Fig. 2a and b indicate that there are significant differences in the absorption and scattering characteristics of the light waves with different thicknesses of the gold film. Furthermore, the peak positions, bandwidths and intensities of the spectral curves all show regular changes. A more detailed analysis of the sensitivity comparison curves in Fig. 2c reveals that the sensitivity of the sensor exhibits an increase followed by a decrease as the thickness of the gold film is increased. It is notable that at a gold film thickness of 38 nm, the sensor sensitivity reaches its peak value. This parameter is thus identified as the optimal solution for subsequent studies.

The subsequent stage is to enter the specialisation phase of the centre aperture radius. The central aperture radius, being the core structural element of photonic crystal fibre, exerts a pivotal influence on the sensor performance by modifying the light propagation path and mode distribution within the fibre. In accordance with the optical theory of fibre optics, the alteration of the aperture size is known to effect a change in the effective refractive index distribution within the fibre's cross-section. This, in turn, has the capacity to regulate the degree of binding and transmission characteristics of the light field. The aforementioned change in optical characteristics is directly related to the sensitivity of the sensor, the resonance wavelength and other core performance indicators.

This study involved a comparative analysis of five typical parameters: 0 μm, 0.05 μm, 0.1 μm, 0.15 μm and 0.2 μm. As illustrated in Fig. 3a, the loss spectrum reveals that the resonance wavelength and loss intensity of the sensor fluctuate considerably with the central aperture radius. Reducing the aperture radius enhances the interaction between the light field and the core material, causing the loss peak to shift towards shorter wavelengths. Conversely, increasing the aperture radius causes the light field distribution to become more dispersed, resulting in significant changes to the shape and position of the loss peak. A more detailed analysis of the performance comparison curves in Fig. 3b shows that the sensing sensitivity is at its best when the central aperture radius is 0.1 μm. Based on the available evidence, 0.1 μm is determined to be the optimal central aperture radius parameter.

The subsequent procedure entailed the optimisation of the radius of the outer stomata. As illustrated in Fig. 4, three parameters were selected for investigation: 1.2 μm, 1.3 μm and 1.4 μm. Fig. 4a and b illustrate the loss spectrum and wavelength sensitivity of the sensor relative to the aperture radius, respectively. The data demonstrate that the wavelength sensitivity of the sensor exhibits a maximum at an outer aperture radius of 1.2 μm, thereby demonstrating superior sensing performance in comparison to other parameters. Consequently, 1.2 μm was identified as the radius parameter of the outer aperture in the subsequent optimisation process Fig. 5.

In conclusion, the optimisation of the polishing depth of H-type photonic crystal fibre is undertaken. The polishing depth is a pivotal parameter that exerts a significant influence

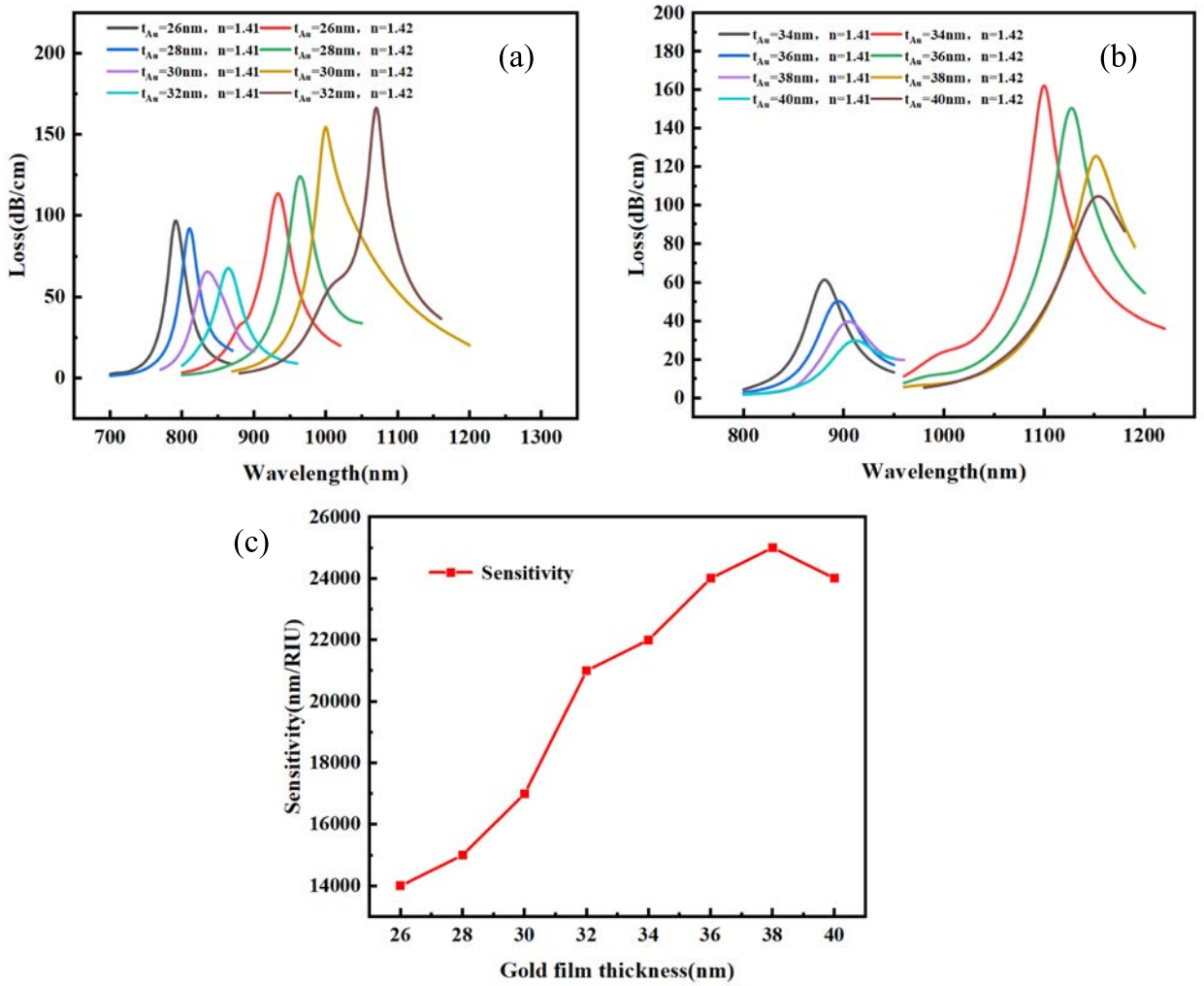

Fig. 2 **a**, **b** Loss spectra for different gold film thicknesses; **c** comparison of sensitivity at different gold film thicknesses

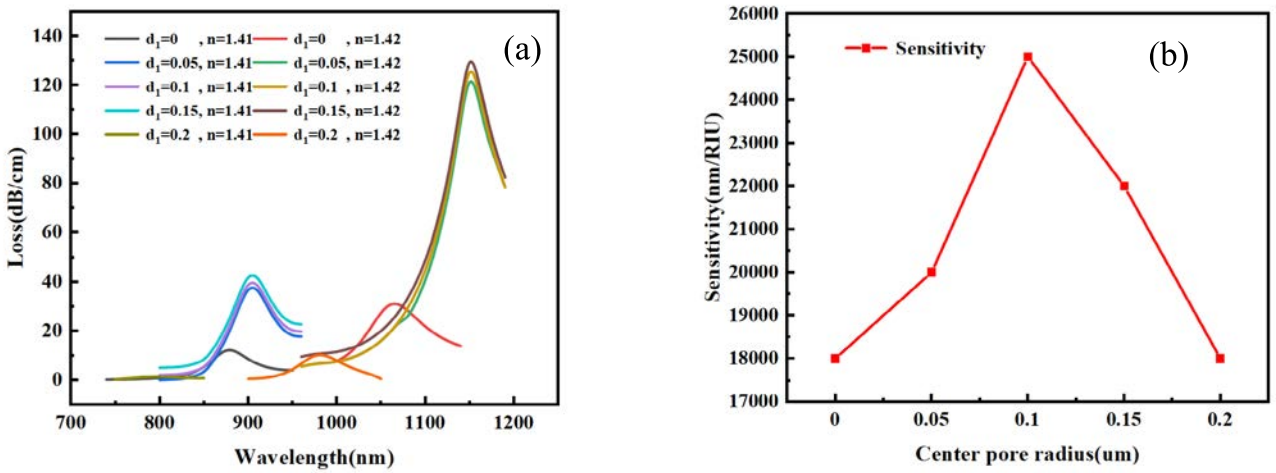

Fig. 3 **a** Loss spectra at different central stomatal radii; **b** comparison of sensitivity at different centre stomatal radii

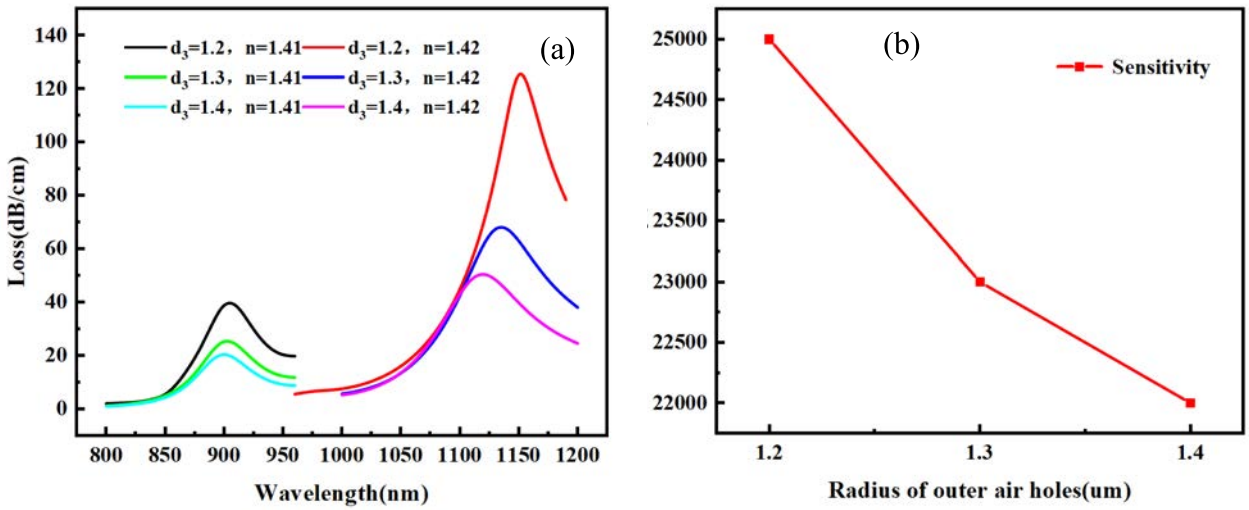

Fig. 4 **a** Loss spectra for different radii of outer air holes; **b** Comparison of sensitivity at different radii of outer air holes

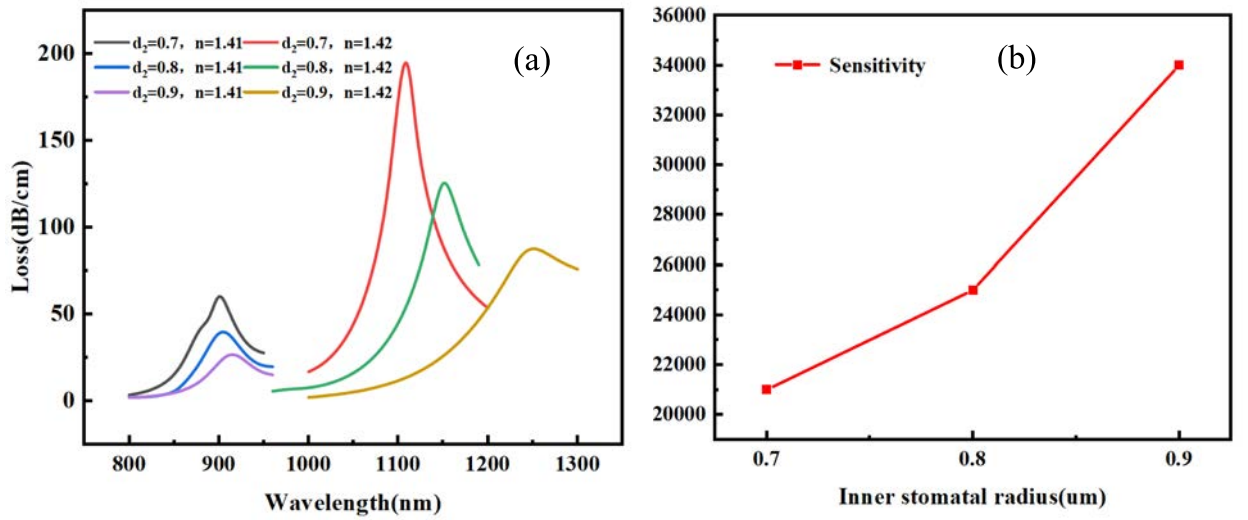

Fig. 5 **a** Loss spectra under different sizes of inner air holes; **b** comparison of sensitivity at different medial stomatal radii

on the optical performance of the sensor. It primarily affects the sensor's sensing capability towards the target material by modifying the distribution characteristics of the abrupt field. Surface plasmon resonance theory posits that alterations in polishing depth result in modifications to the interaction region between the fibre surface and the external environment. These alterations directly impact the coupling efficiency of the swiftly passing field and the external material, exerting a substantial influence on the sensitivity and detection range of the sensor. The results of the simulation analysis demonstrate that a specific grinding depth threshold exists. Exceeding this threshold results in the sensor's inability to stimulate the SPR effect, thereby leading to the failure of the sensing function.

In light of the theoretical analysis and simulation conclusions outlined above, two polishing depths, 5 μm and 5.5 μm, have been selected for comparative study in this stage of the research. As demonstrated in Fig. 6, the comparison data indicates that the sensor's sensitivity attains its optimal level at a polishing depth of 5 μm. In comparison with a polishing depth of 5.5 μm, the former exhibits substantial advantages with respect to the excitation efficiency of the SPR effect and the intensity of the interaction between light and the material. Consequently, 5 μm is designated as the polishing depth parameter for the ensuing study.

Following a series of optimisation procedures, the fundamental structural parameters of the photonic crystal fibre

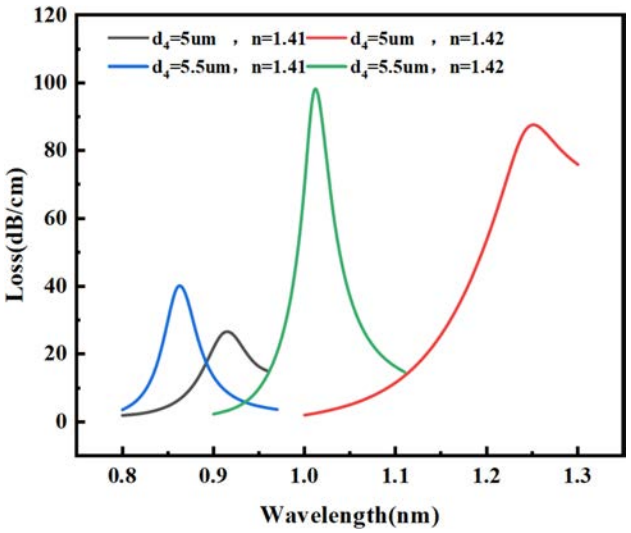

Fig. 6 Loss spectra at different depths of abrasion

optic sensor have been ascertained. The thickness of the gold layer (t_{Au}) has been established at 38 nm, the radius of the central aperture (d_1) at 0.1 μm, the radius of the inner aperture (d_2) at 0.9 μm, and the radius of the outer aperture (d_3) at 1.2 μm, depth of polishing (d_4) 5 μm.

The wavelength range is constrained to the interval between 500 and 1600 nm, in comparison with the standard wavelength range of fibre optic sensors. The spectral region in which the majority of fibre optic sensors exhibit excellent transmission characteristics, high sensitivity and optimal performance is covered by this band. Through the implementation of systematic simulation, it has been determined that the designed sensors demonstrate optimal sensing performance when the operating wavelength is within the range of 570–1300 nm. The key indexes of the sensors, including loss spectral characteristics and wavelength sensitivity, are also found to be within the optimal state. This provides a reliable parameter basis for the subsequent experimental validation and practical application of the sensors.

As postulated by the surface plasmon resonance theory, a unique energy coupling mechanism is triggered at the interface of the gold film medium in the photonic crystal fibre sensor. This is the result of the fundamental mode in the fibre core meeting the phase-matching condition with the surface dissociative polariton (SPP) mode. At this time, the electromagnetic field of the light wave excites the free electrons on the metal surface, thereby generating collective oscillations and forming SPP modes propagating along the interface. A portion of the energy in the fundamental mode is transferred to the SPP modes through the swift field coupling, resulting in significant energy loss within the fibre core.

In the process of characterising the energy loss of the fundamental mode, the constrained loss of the fundamental mode can be quantified by a specific formula, the expression of which is as follows [24]:

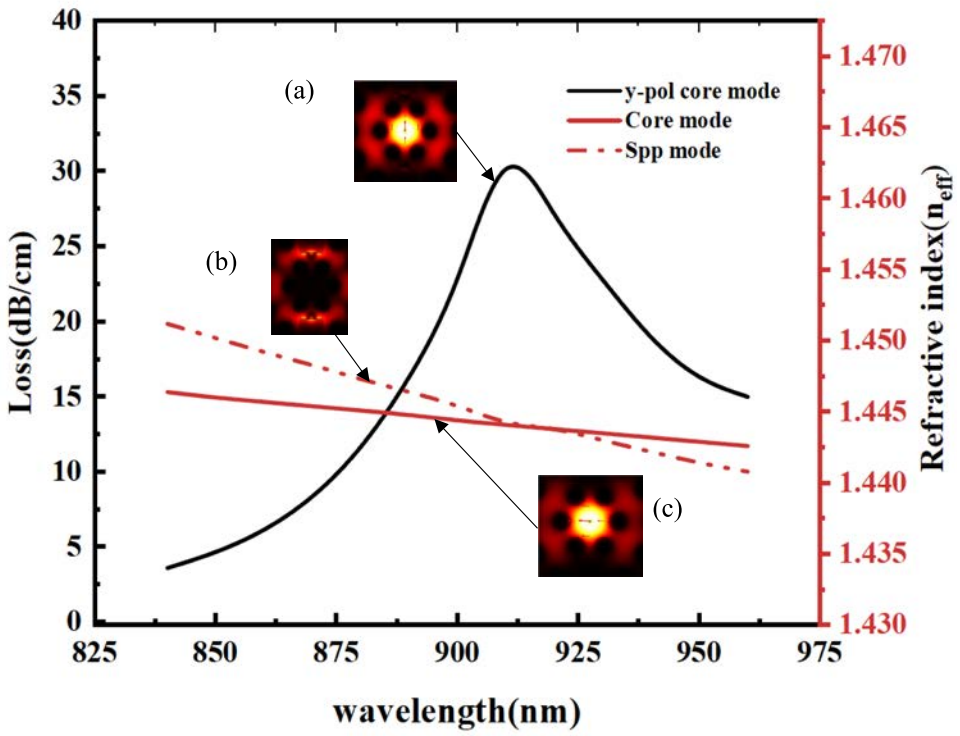

Fig. 7 Base mode and SPP mode loss curves of the sensor for refractive index $n = 1.41$: **a** fundamental modes in y-polarisation; **b** SPP mode; **c** SPR mode

$$CL(dB/cm) = 8.686 \times \frac{2\pi}{\lambda} \times \mathrm{Im}\left(n_{eff}\right) \times 10^4 \quad (3)$$

In the context of optical fibre theory, the wavelength of the incident light, denoted by λ, and the imaginary part of the effective refractive index of the optical fibre fundamental mode, denoted by $\mathrm{Im}(n_{\mathrm{eff}})$, are fundamental parameters.

As illustrated in Fig. 7, the dispersion profile and loss profile of the sensor surface plasmon resonance are shown for an analyte refractive index of $n = 1.41$. As the incident wavelength increases, the effective refractive indices of the fundamental mode and the real part of the SPP mode both tend to decrease and intersect at a wavelength of 915 nm, which marks the phase-matching condition. When the wavelength is less than 915 nm, the effective refractive index of the fundamental mode is lower than that of the SPP mode. In accordance with the SPR effect, the energy in the core is transferred to the metal surface through abrupt field coupling, resulting in a significant increase in core energy loss. Conversely, when $\lambda > 915$ nm, the effective refractive index of the fundamental mode is lower than that of the SPP mode.

When the wavelength is greater than 915 nm, the effective refractive index of the fundamental mode is higher than that of the surface plasmon polariton (SPP) mode. This results in the energy on the metal surface starting to be transferred back to the core in the reverse direction. This, in turn, leads to a decrease in the energy loss of the core.

The insets (a) and (b) illustrate the electric field distributions of the fundamental mode and the SPP mode of the core, respectively, and the inset (c) demonstrates the electric field distributions of the two in the resonant coupling state. A comparison of insets (a) and (c) reveals that in the absence of the resonance condition, the incident light energy is predominantly confined to the interior of the fibre core. Conversely, when resonant coupling occurs,

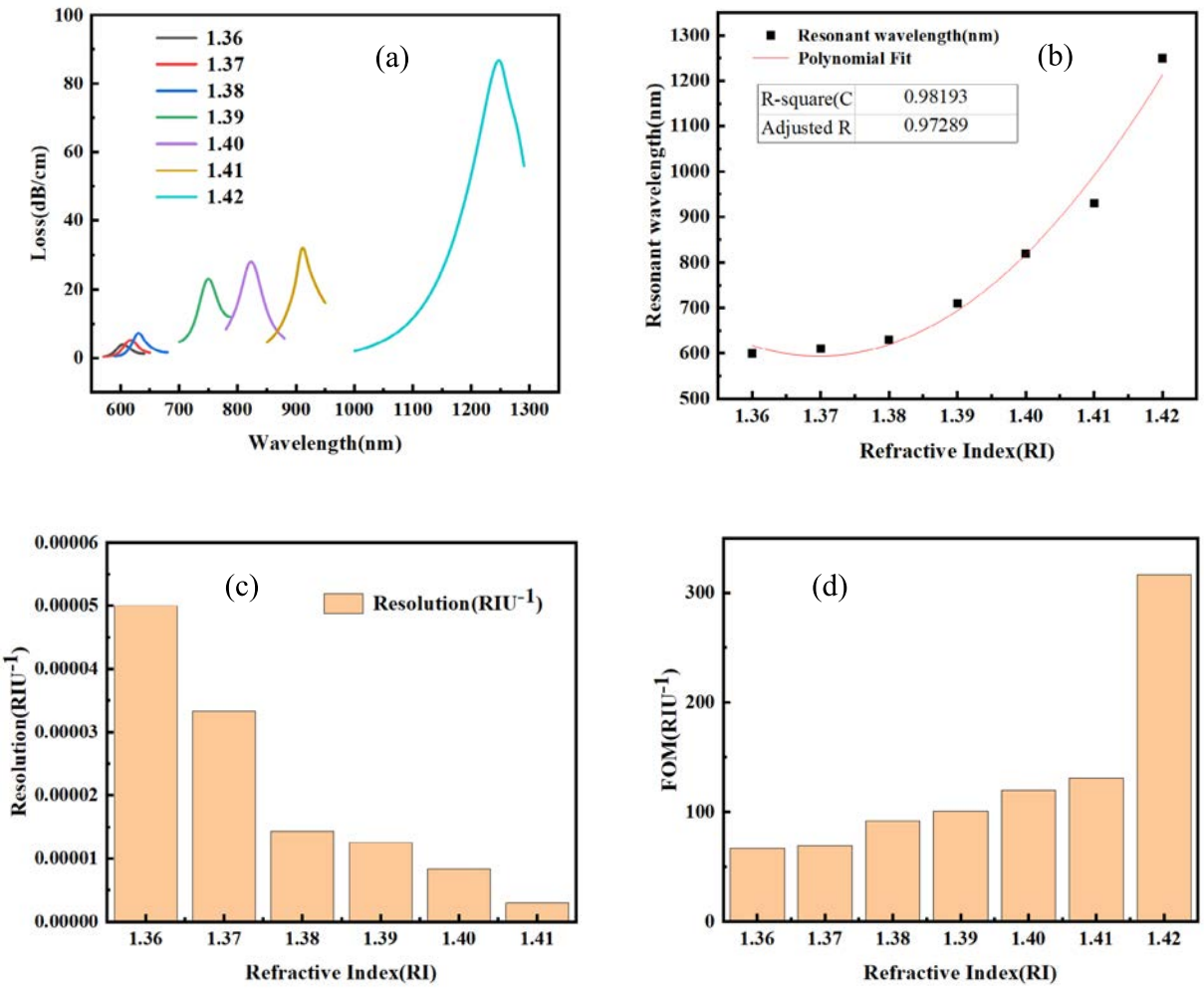

Fig. 8 **a** Loss spectra for RIs between 1.36 and 1.42; **b** polynomial fit of the resonance wavelengths; **c** resolution of the sensor; **d** FOM for different analytes' RI

Table 2 Comparison of the performance of our and similar sensors reported recently

Refs.	Detection Range	WS (nm/RIU)	R(RIU)	Structure Diagram
[27]	1.38-1.42	22100	4.5×10^{-6}	
[28]	1.33-1.34	20000	5×10^{-6}	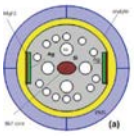
[29]	1.375-1.4	20000	5×10^{-6}	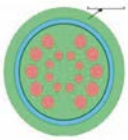
[30]	1.31-1.35	25000	4×10^{-6}	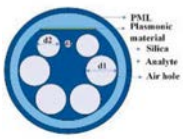
This work	1.36-1.42	34000	2.94×10^{-6}	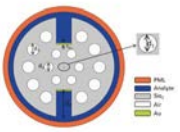

a portion of the energy is successfully transferred to the metal surface. This observation provides a tangible validation of the energy transfer process initiated by the SPR effect, thereby establishing the foundation for visualising the sensor's operational mechanism.

The wavelength sensitivity, which is a significant performance indicator of the sensor, can be calculated using Eq. (4). This equation describes the variation of the resonance wavelength with the refractive index [25]:

$$S(\lambda, n) = \frac{\Delta\lambda}{\lambda n}(nm/RIU) \tag{4}$$

It is imperative to note that the term "$\Delta\lambda$" denotes the discrepancy in resonance wavelength, while "Δn" signifies the variation in the change in refractive index of the analyte.

Wavelength resolution (R), as a core parameter of sensor performance, comprehensively characterises the optical sensing properties of a sensor. This parameter intuitively reflects the sensitivity of the sensor to small wavelength shifts and its ability to resolve small changes in the refractive index of the analysed substance. It is important to note that a lower value of wavelength resolution means that the sensor has a smaller perception threshold for changes in the refractive index of the analysed substance and is able to detect smaller changes in physical quantities, which are calculated as follows [26]:

$$R = \frac{\Delta n_a \times \Delta\lambda_{min}}{\Delta\lambda_{peak}} = \frac{\Delta\lambda_{min}}{S_\lambda}(RIU) \tag{5}$$

In addition to wavelength resolution, the quality factor (FOM), also known as the figure of merit, is an equally important indicator of instrument performance. The purpose of this parameter is to visualise the instrument's ability to resolve weak optical signals. This is achieved by quantifying the ratio between wavelength sensitivity

Table 3 Sensing performance parameters of the sensor

Refractive index of the analyte	Resonance wavelength (nm)	Wavelength sensitivity (WS, nm/RIU)
1.36	600	1800
1.37	618	2000
1.38	638	9600
1.39	734	10,000
1.40	834	8300
1.41	917	34,000
1.42	1257	——-

and half-width (FWHM). It is generally accepted that a larger FOM value indicates that the instrument is capable of achieving higher detection accuracy and lower detection limit under equivalent conditions. The mathematical expression for this relationship is as follows [21]:

$$FOM = \frac{S_\lambda}{FWHM}\left(RIU^{-1}\right) \tag{6}$$

As illustrated in Fig. 8a, the loss spectral characteristics of the sensor are demonstrated. It has been established that the loss spectrum demonstrates a substantial increase in redshift with rising peaks as the analyte refractive index rises. This phenomenon is attributed to the positive correlation between the effective refractive index of the surface plasmon polariton mode and the analyte refractive index, while the effective refractive index of the fibre optic substrate mode remains relatively stable.

As illustrated in Fig. 8b, the polynomial fitting results for the resonance wavelength demonstrate a high degree of correlation, as evidenced by a coefficient of determination (R^2) of approximately 0.98, which signifies a robust fit. According to Eq. (4), the sensor demonstrates optimal sensing performance within the RI detection interval of 1.36–1.42, exhibiting a maximum sensitivity of 34,000 nm/RIU and an average sensitivity of 10,833.3 nm/RIU. Furthermore, the sensor demonstrates a high level of resolution, calculated according to Eq. (5), with a minimum resolution of 2.94×10^{-6} (Fig. 8c). As demonstrated in Fig. 8d, the quality factor (FOM) is calculated to be 316 RIU^{-1} at RI = 1.42, as per Eq. (6). The data presented herein demonstrate that the sensor exhibits significant advantages in terms of sensing performance and demonstrates considerable potential for application.

In order to visualise the performance advantages of the present sensor, a systematic comparison of its key performance parameters with those of similar PCF-SPR sensors in the literature is presented in Table 2. The results show that, compared with the reported research results, the H-type PCF-SPR sensor with annular aperture array designed in this study exhibits significant advantages in the core indexes such as sensitivity, detection range and resolution, which fully confirms its excellent sensing characteristics and technological innovation. Table 3 shows the sensing performance parameters of the sensor, which can used to calculate the average sensitivity of 10,833.3 nm/RIU.

Conclusion

This study presents a highly sensitive PCF-SPR sensor with H-shaped annular hole array structure, and its coupling characteristics and sensing performance were analysed using the finite element method. By systematically optimising the structural parameters, the sensing sensitivity of the sensor was remarkably increased. In the refractive index range of 1.36 to 1.42, a maximum wavelength sensitivity of 34,000 nm/RIU and an average sensitivity of 10,833.3 nm/RIU are achieved, coresponding to a resolution of 2.94×10^{-6} RIU. This sensor can be used to monitor and analyse biological molecules, cells and biomedical field for disease diagnosis. For instance, the sensor can monitor dynamic changes in the refractive index of cells such as Basal, Hela, Jurkat and PC12 in real time, providing reliable evidence for the early diagnosis of cancer.

Author Contributions Chao Liu: Conceptualization, Writing- Reviewing and Editing. Fengrui Yang: Conceptualization, Data Curation, Methodology, Software, Writing- Original Draft. Wei Liu: Formal analysis. Jianxin Wang: Methodology, Supervision. Jingwei Lv: Formal analysis. Famei Wang: Formal analysis. Zao Yi: Funding acquisition, Validation. Qiang Liu: Software, Validation. Paul K. Chu: Resources, Project administration.

Funding This work was jointly supported by the Natural Science Foundation of Guangdong Province (2022A1515110971), the Heilongjiang Provincial Natural Science Foundation of China (JQ2023F001), the National Natural Science Foundation of China (12304480), the Natural Science Foundation of Heilongjiang Province (LH2021F007), the China Postdoctoral Science Foundation funded project (2020M670881), and the City University of Hong Kong Donation Research Grants (DON-RMG 9229021 and 9220061).

Data Availability No datasets were generated or analysed during the current study.

Declarations

Competing interests The authors declare no competing interests.

References

1. Wang J, Xili Lu, Mi C, Yin Q, Lv J, Yang L, Liu W, Yi Z, Liu Q, Chu PK, Liu C (2024) Ultra-high sensitivity photonic crystal fiber sensor based on dispersion turning point sensitization of surface plasmonic polariton modes for low RI liquid detection. Opt Express 32:32895–32908
2. Abdelghaffar M, Gamal Y, El-Khoribi RA et al (2023) Highly sensitive V-shaped SPR PCF biosensor for cancer detection. Opt Quant Electron 55:472
3. Bing PB, Liu Q, Wu GF, Yuan S, Li ZY, Du HL et al (2022) A plasmonic sensor based on D-shaped dual-core microchannel photonic crystal fiber. Plasmonics 17(4):1471–1478
4. Islam MR, Iftekher ANM, Meraz MHI et al (2023) Design of a dual arrow shaped and dual plasmonic material compatible SPR PCF sensor. Opt Quant Electron 55:1125
5. Hasan MS, Kalam MAE, Faisal M (2024) PCF based four-channel SPR biosensor with wide sensing range. IEEE Trans Nanobiosci 23(2):233–241
6. Majeed MF, Ahmad AK (2024) Design and analysis of a dual-core PCF biosensor based on SPR for cancerous cells detection. Opt Quant Electron 56:1030

7. Liu W, Shi Y, Yi Z, Liu C, Wang FM, Li XL, Lv JW, Yang L, Chu PK (2021) Surface plasmon resonance chemical sensor composed of a microstructured optical fiber for the detection of an ultra-wide refractive index range and gas-liquid pollutants. Opt Express 29(25):40734–40747
8. Krishnan P, Khamaru A, Kumar A (2025) MXene coated concave shaped microchannel PCF SPR biosensor for the detection of HIV and sickle cell anaemia. Opt Quant Electron 57:270
9. Liu W, Liu C, Wang JX, Lv JW, Lv Y, Yang L, An N, Yi Z, Liu Q, Hu CJ, Chu PK (2023) Surface plasmon resonance sensor composed of microstructured optical fibers for monitoring of external and internal environments in biological and environmental sensing. Results Phys 47:106365
10. Akter S, Abdullah H (2024) Design and investigation of high-sensitivity PCF SPR biosensor for various cancer cells detection using a gold-coated circular-shaped structure". Plasmonics 31:1–1
11. Meng F, Wang H, Fang D (2022) Research on D-shape open-loop PCF temperature refractive index sensor based on SPR effect. IEEE Photo J 14(3):1–5 Art no. 5727605
12. Wang J, Pei L, Wu L et al (2020) A polarization-independent SPR sensor based on photonic crystal fiber for low RI detection. Plasmonics 15:327–333
13. Hu LC, Li JS, Li SG, Zhao YY, Yin ZY, Li KF et al (2023) A dual-core two-parameter of RI and temperature photonic crystal fiber sensor based on the SPR effect. Plasmonics 19:1667–78
14. Jiao S, Gu S, Yang H et al (2018) Highly sensitive dual-core photonic crystal fiber based on a surface plasmon resonance sensor with a silver nano-continuous grating[J]. Appl Opt 57(28):8350–8358
15. Gandhi MA, Chu S, Senthilnathan K, Babu PR, Nakkeeran K (2019) Li Q "Recent advances in plasmonic sensor-based fiber optic probes for biological applications." Appl Sci 9(5):949
16. Luo W, Meng J, Li X, Xie Q, Yi D, Wang Y, Hong X (2021) Temperature effects on surface plasmon resonance sensor based on side-polished D-shaped photonic crystal fiber. Measurement 181:09504
17. Zhang Z, Yin Z, Li S, Linchuan Hu (2024) Cascaded dual-parameter SPR fiber sensor for RI and pH simultaneous detection based on Ag film and an Ag/self-assembled nanofilm structure. Opt Express 32:33330–33343
18. Tuaimah AM, Taher HJ, Tahhan SR et al (2023) Plasmonic D-shaped bimetallic coating refractive index sensor. Plasmonics 18:2393–2404
19. Fei Y, Luo B, An M et al (2025) A highly efficient D-shaped dual-core PCF-SPR sensor coated with ITO film for refractive index detection. Plasmonics 20:1379–1393
20. Luo B, An M, Hu T et al (2024) Dual-channel surface plasmon sensor based on photonic crystal fiber for low refractive index detection. Opt Quant Electron 56:1059
21. Jabin MA, Ahmed K, Rana MJ, Paul BK, Islam M, Vigneswaran D (2019) Uddin MS "Surface plasmon resonance based titanium coated biosensor for cancer cell detection." IEEE Photonics J 11(4):1–10
22. Bing P, Sui J, Wu G et al (2020) Analysis of dual-channel simultaneous detection of photonic crystal fiber sensors. Plasmonics 15:1071–1076
23. Nashaye Rafi H, Kaysir R, Islam J (2020) Air-hole attributed performance of photonic crystal fiber-based SPR sensors. Sens Bio-Sens Res 29:100364 ISSN 2214-1804
24. Liu Q et al (2020) The biochemical sensor based on liquid-core photonic crystal fiber filled with gold, silver and aluminum. Opt Laser Technol 130:106363
25. Wang Qi, Wang B (2018) Sensitivity enhanced SPR immunosensor based on graphene oxide and SPA co-modified photonic crystal fiber. Opt Laser Technol 107:210–215
26. Li M, Peng L, Zhou G, Li B, Hou Z, Xia C (2017) Design of photonic crystal fiber filter with narrow width and single-polarization based on surface Plasmon resonance. IEEE Photo J 9(3):1–8 Art no. 5700108
27. Zhang Q, Li W, Ren Q, Zheng J, Xie Q, Wang X (2022) A D-type dual side-polished, highly sensitive, plasma refractive index sensor based on photonic crystal fiber. Front Phys 10:1008784
28. Manickam P, Senthil R (2022) Numerical investigation of side-polished SPR PCF sensor for urine analysis. Plasmonics 17:2023–2030
29. Kumar S, Kumar D (2022) Sensitivity measurement based on the refractive index detection of dual-coated PCF SPR sensor. Mapan 37:435–441
30. Divya J, Selvendran S (2025) Performance evaluation of D-shaped photonic crystal fiber based SPR sensors with different plasmonic materials: a comparative analysis. Res Eng 26:104715 ISSN 2590-1230